International Journal of Thermofluid Science and Technology (2024)
Volume 11, Issue 2, Paper No. 110202
https://doi.org/10.36963/IJTST.2024110202

Research Article

Numerical study of natural convection of Bingham fluid using a flexible fin

Hanaa Derraz [1], Bouzit Mohamed [1], Mokhefi Abderrahim[2] Bencherif Atika [1], Meriem Toumi[1]

[1] *LSIM, Faculty of Mechanical Engineering, University of Science and Technology of Oran, Mohamed Boudiaf, El Mnaouar, Oran, Algeria*
[2]*Mechanics, Modeling and Experimentation Laboratory L2ME, Faculty of Sciences and Technology, Bechar University B.P.417, 08000, Bechar, Algeria*

ATICLE INFO

Received: 10 Jan. 2024;
Received in revised form:
03 Mar. 2024;
Accepted: 20 Apr. 2024;
Published online:
23 Apr. 2024

Keywords:
Natural convection
Bingham plastic fluid
FSI
Heat transfer
Nusselt number

ABSTRACT

This research focuses on the analysis of the flow and heat transfer inside a square cavity containing a Bingham plastic fluid. The cavity undergoes heating on its left side, where a flexible and elastic fin is positioned at the center of this heated wall. Cooling takes place on the right side of the cavity, while the upper and lower walls are well-insulated. The equations governing the complex interaction between the fluid and the flexible fin are accurately solved using an arbitrary Lagrangian-Eulerian approach, in conjunction with the finite element methodology. This study concentrates on the impact of the flexible fin on heat transfer in the context of unsteady natural convection of a complex fluid with a yield stress inside a square cavity. The considered parameters include the variation of the Rayleigh number in the range of 10^3 to 10^5, the modification of the elasticity modulus between 5×10^{10} and 5×10^{11}, the fin length *(Lc)* from 0.004 to 0.0073, the Prandtl number *(Pr)* from 0.71 to 100, and the variation of the Bingham number from 0 to 20. To provide a comprehensive understanding of the observed thermal and fluidic phenomena, results will be displayed in the form of isothermic contours and streamlines, accompanied by Nusselt number *(Nu)* and maximum stress (σ_{max}) curves. Observations indicate a significant improvement in the Nusselt number in the absence of a yield stress (*Bn=0*), reaching its maximum at *($Ra = 10^5$)*. Conversely, the variation of the elasticity modulus shows negligible influence. As the yield stress *(Bn)* increases, it begins to dominate the flow by nullifying the buoyancy-induced current, reaching a constant value for *(Bn=20),* corresponding to the conduction limit.

1. Introduction

The study of natural convection flow and heat transfer within various cavities filled with non-Newtonian fluids is an interdisciplinary subject of significant interest to researchers in the field of fluid dynamics.

Corresponding e-mail: hanaa.derraz@univ-usto.dz

Nomenclature

B	Coefficient of the volumetric thermal expansion	*Greek symbols*	
Bn	Bingham's number	α	Coefficient of the thermal diffusivity
Et	Dimensional Young's modulus	μ	The fluid's dynamic viscosity
F_v	Vector of volume force	ρ	Density
g	Gravity vector	$\tau_{ij,}\ \tau_0$	Extra stress tensor, Yield stress of fluid
L	Characteristic size	τ	Dimensionless time
Nu	Nusselt number	σ	The solid stress tensor
N	Dimensionless normal vector	θ	Dimensionless temperature
n	Normal vector	η	Apparent viscosity, dimensionless
Pr	Prandtl number	$\dot{\gamma}$	Rate of strain tensor
Ra	Rayleigh number	Ψ	Stream function
t	Time	ψ	Dimensionless stream function
T	Temperature field	*Subscripts*	
u,v	velocity components	*avg*	Average
U,V	Dimensionless velocity components	*c*	Cold temperature
		h	Hot temperature
x,y	Cartesian coordinates	*s*	solide
X,Y	Dimensionless cartesian coordinates	*f*	fluid
		*	dimensionless for variables and parameters

Natural convection phenomena play a crucial role in numerous engineering and applied science domains, such as electronic equipment cooling, geothermal applications, material processing, heat exchangers, lubrication, solar collectors, and more. Bingham plastic fluids are an effective method to improve the performance and efficiency of many industrial and environmental systems, so it is essential to understand the rheological properties of these fluids in cavities.

Numerous scientific studies have investigated natural convection heat transfer using a flexible fin, focusing on the fluid-structure interaction problem inside the cavity [1-6]. They found that flexible fins offer higher bends for dilatant fluids, while rigid fins offer better stress resistance. Larger baffles increase flow resistance and constrain heat transfer, but strain increases, and fluctuating heaters reduce heat transfer and Nusselt number. Each study has explored the impact of fluid-structure interaction on temporary free convection in a square cavity filled with air, involving a flexible horizontal baffle [7]. The results show that the bend of the elastic components is reduced, and the saved energy within the elastic material is transferred to the circulating fluid, reinforcing the convective flow for high Rayleigh numbers.

A numerical study of unstable natural convection in a heated slanting enclosure with an elastic oscillating fin established on the lowest adiabatic wall was conducted [8]. The study reveals that the flexible fin's inclination angle significantly impacts fluid flow and heat transfer in an oblique cavity, with increased Young's modulus intensifying convective flow and decreasing Nusselt number for $t > -4$.

In addition, a smoothed particle element method (SPEM) for simulating fluid-structure interaction problems with permeable surfaces was developed [18,19]. It also demonstrates the efficient coupling of ESFEM with SPH through a virtual particle scheme.

However, the unsteady natural convection inside diverse cavities using MHD flow, such as square cavities [14-16] and circular cavities [17], reveals that the magnetic field presence affects temperature, membrane shape, and heat transfer in cavities. The Hartmann number and

magnetic field orientation angle influence membrane shape and heat transfer, with nanoparticle concentration affecting flow strength.

The problem of unsteady natural convection inside enclosures using oscillating fins has been studied in the literature [11-13]. These studies show that at Ra > 10^5, flow transitions to a fully periodic regime, with irregular behavior concerning time. Fluid yield stress defers loss of steadiness to higher Rayleigh numbers. Maximum heat transfer enhancement occurs at suitable parameters between aperture size and fin oscillating direction.

In many published works concerning porous layers or mediums in enclosures filled with non-Newtonian fluid, it has been discovered that the overall amount of heat transfer increases exponentially with the rise of the oscillation amplitude. An enhancement in the heat transfer rate of 3.4% might result from an oscillation amplitude of 0.1, while the Darcy number shows a higher average Nusselt number compared to the Darcy-Forchheimer model for all studied Rayleigh numbers [9-10].

The transitory mixed convection within a square enclosure was studied [40-41]. They found that cavities with flexible baffles have the highest average Nusselt number, with a significant influence of the elasticity value on the heat transfer rate at small amplitude oscillations, in contrast to cavities with rigid baffles and without baffles.

On the other hand, much literature concerning heat transfer by laminar free convection from an immersed circular cylinder in Bingham plastic fluids, square cross-sectioned cylindrical annular enclosures, and rectangular enclosures have been investigated [20-26]. The enhanced heat transfer proportion due to increased Bn could be more than compensated for by the enhanced Rayleigh number, with the Nusselt number showing an inverse dependence. Therefore, the problem of fluid-structure interaction of viscoplastic fluids inside different shapes of enclosures, such as a square cavity [27], C-shaped enclosure [28], a heated sphere in tubes [29], and cylindrical enclosure [30], has been explored. These studies reveal that the yielded/unyielded sections and streamlines intensify with increasing buoyancy ratio, Rayleigh number Ra, Lewis number, and wavy baffle amplitude while decreasing with wave number, while the local Nusselt improves with Ra amplification, and average entropy and Bejan number reach higher values at low Ra.

The effects of fluid temperature-structured viscosity, yield stress, and viscous dissipation on natural convection from an isothermal surface in a Bingham plastic fluid were studied [31]. It was found that the average Nusselt number decreases regularly with the Bingham number from its maximum value in Newtonian fluids (Bn = 0) to its minimum value proportional to the conduction limit.

Although the natural convection of other viscoelastic fluids, like Casson fluid [32] and Herschel-Bulkley fluid [33-35], has also been investigated. These literatures show that heat transfer increases with the Hartman number and magnetic intensity for cold walls, while the Rayleigh number and Casson viscoelastic fluid parameters increase velocity profiles. Also, the increased generalized Bingham number leads to increased unyielded regions, and heat transfer is more

pronounced for weak values and high fluid flow index, and viscous dissipation significantly modifies flow and heat transfer structures.

The distinction between precise analytical solutions delineating natural and thermocapillary convection in horizontal single-layer and double-layer devices, including Newtonian and viscoelastic fluids, was studied [35].

In other studies, regarding the mixed convection of Newtonian fluid inside many enclosures such as a cavity channel [36], a square cavity having two inlet and outlet openings [37-38], and a square cavity having a flexible side wall [39], the heat transfer enhancement in a trapezoidal cavity using non-Newtonian power-law fluids was performed[42], and their study reveals that stiff fins have higher Nusselt numbers at Re = 300, with higher values for shear-thickening fluid and shear-thinning fluid at low Ri numbers, and fluttering occurs at high Ri and Re numbers. Double-diffusive convection of power-law

nanofluids within rectangular enclosures using the regularized lattice Boltzmann method was investigated [43]. The results show that increasing nanoparticle volume fraction increased the average Nusselt number but reduced the average Sherwood number, while the average Nusselt and Sherwood numbers decreased with the increasing power-law index.

The influence of temperature-dependent characteristics on the natural convection of nanofluids in rectangular cavities with sinusoidal temperature distribution using the lattice Boltzmann method was performed [44-45], and the results show an optimal volume fraction for maximum heat transfer enhancement, which increases slightly with nanoparticle diameter and remarkably with temperature, and the average Nusselt number decreases with the power-law index and increases with temperature.

As mentioned earlier, previous studies have suggested various directions to deepen the understanding of heat transfer properties and flow patterns in convection configurations involving elastic deflectors and complex fluids.

This recent study provides new perspectives on natural convection inside square cavities equipped with elastic deflectors filled with a Bingham-type complex fluid. It analyzes parameters such as Rayleigh number (Ra), elasticity modulus (Et), Prandtl number (Pr), Bingham number (Bn), and the length of the elastic deflector to evaluate their impact on heat transfer. This topic presents promising prospects for future applications. The analysis includes streamline visualization, isotherm profiles, and the determination of average Nusselt numbers and σmax to present the results.

2. Modeling approach:

2.1 Description of physical model

The geometry studied in this research, illustrated in Figure 1, consists of a 2D square cavity of length noted L, filled with a Bingham fluid. The left and right walls of the cavity are maintained at high temperature Th* and cold temperature Tc*, respectively, while the other walls remain adiabatic. In addition, an elastic flexible fin, with a thickness of t_{fin}, is fixed in the central part of the left wall, and this fin is also considered adiabatic. Due to natural convection, the pushing force causes the flexible fin to bend. The no-slip condition is applied to all cavity walls, including the outer walls and fin surfaces. Temperature variations are assumed to be partial. With the exception of density, all thermophysical properties are considered to be independent of temperature.

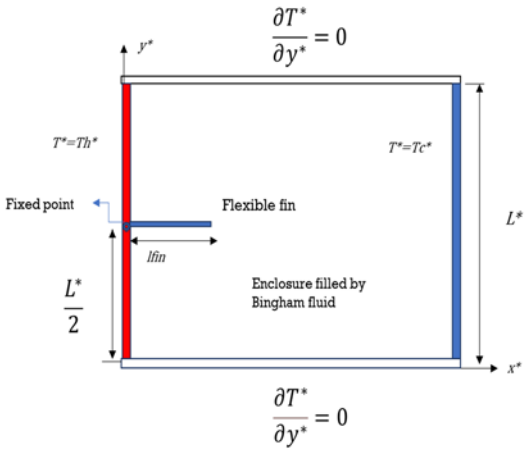

Fig . 1 Physical model of the problematic

2.2 Mathematical equations

2.2.1 Mathematical dimensional equations

The dimensional equations modeling the hydrodynamic, thermal and elastic characteristics of the problem are obtained as follows:

Masse balance

$$\frac{\partial u}{\partial x}+\frac{\partial v}{\partial y}=0 \qquad (1)$$

Momentum balance:

$$\rho_f\left(\frac{\partial u}{\partial t}+u\frac{\partial u}{\partial x}+v\frac{\partial u}{\partial y}\right)= -\frac{\partial p}{\partial x}+\left(\frac{\partial \tau_{xx}}{\partial x}+\frac{\partial \tau_{xy}}{\partial y}\right) \qquad (2)$$

$$\rho_f\left(\frac{\partial v}{\partial t}+u\frac{\partial v}{\partial x}+v\frac{\partial v}{\partial y}\right)=-\frac{\partial p}{\partial y}+ \left(\frac{\partial \tau_{xy}}{\partial x}+\frac{\partial \tau_{yy}}{\partial y}\right)+\rho_f g\beta(T-T_c) \qquad (3)$$

The energy equation for the fluid:

$$\rho_f Cp_f \left(\frac{\partial T}{\partial t} + u\frac{\partial T}{\partial x} + v\frac{\partial T}{\partial y} \right) = k_f \left(\frac{\partial^2 T}{\partial x^2} + \frac{\partial^2 T}{\partial y^2} \right) \quad (4)$$

Structural displacement of the flexible fin:

$$\rho_s \frac{\partial^2 d_{sx}}{\partial t^2} - \left(\frac{\partial \sigma_{xx}}{\partial x} + \frac{\partial \sigma_{xy}}{\partial y} \right) = F_{vx} \quad (5)$$

$$\rho_s \frac{\partial^2 d_{sy}}{\partial t^2} - \left(\frac{\partial \sigma_{yx}}{\partial x} + \frac{\partial \sigma_{yy}}{\partial y} \right) = F_{vy} \quad (6)$$

ds denote the displacement vector of the fin
The Neo-Hookean solid model is applied to express the stress tensor

The tensor σ is given by:

$$\boldsymbol{\sigma} = \mathbf{J}^{-1}\mathbf{F}\mathbf{S}\mathbf{F}^{T} \quad (7\text{-a})$$

With S representing the second Piola-Kirchhoff stress tensor. It is given by :

$$\boldsymbol{S} = 2\mu_s \boldsymbol{G} + \lambda tr(\boldsymbol{G})\boldsymbol{I} \quad (7\text{-b})$$

With G being the tensor of non-linear deformation. It is given by:

$$\boldsymbol{G} = \frac{1}{2}\left(\boldsymbol{F}^{T}\boldsymbol{F} - \boldsymbol{I}\right) \quad (7\text{-c})$$

The tensor F represents the deformation gradient:

$$\boldsymbol{F} = \boldsymbol{I} + \nabla \vec{w}^{T} \quad (7\text{-d})$$

With λ and μ representing the Lamé coefficients. They are respectively given by:

$$\lambda = \frac{\nu E}{(1+\nu)(1-2\nu)} \quad (8)$$

$$\mu_s = \frac{E}{2(1+\nu)} \quad (9)$$

With ν being the Poisson's ratio and E representing the Young's modulus of the structure.
The energy equation for the flexible fin:

$$\rho_s Cp_s \left(\frac{\partial T_s}{\partial t} \right) = k_s \left(\frac{\partial^2 T_s}{\partial x^2} + \frac{\partial^2 T_s}{\partial y^2} \right) \quad (10)$$

P and T are the pressure of the fluid and temperature of the solid/ fluid, respectively, g the gravity acceleration. Fv indicates the body force imposed on the flexible fin. ρ indicates the density where *f* and *s* mention to the fluid and solid, respectively. *αf* is thermal diffusivity of the fluid, *αs* thermal diffusivity of the solid and β shows the volumetric thermal expansion coefficient of the fluid

For a Bingham plastic fluid, the extra stress tensor, τ_0 is written as follows:

$$\tau_{ij} = \tau_0 + \mu_B \dot{\gamma} \text{ if } \left|\tau_{ij}\right| \succ \left|\tau_0\right| \qquad \dot{\gamma} = 0 \text{ if } \left|\tau_{ij}\right| \le \left|\tau_0\right| \quad (11)$$

With: μ_B is The viscosity of Bingham fluid and μ_p is yielding viscosity

$$\tau_{ij} = \frac{1}{2}\mu_B \left(\frac{\partial u_i}{\partial x_j} + \frac{\partial u_j}{\partial x_i} \right)$$

Equation (11) can be simplified using the Papanastasiou model for flow

$$\mu_B = \mu_p + \tau_y \dot{\gamma}^{-1}(1 - e^{-m\dot{\gamma}}) \quad (12)$$

With, Eqs. (11) and (12) can be rewritten in their dimensionless form as follows

$$\tau^*_{ij} = \left(1 + \frac{Bn}{\left|\dot{\gamma}\right|} \right) \dot{\gamma} \quad (13)$$

The viscosity scalar for a Bingham fluid:

$$\mu_B^* = \left(1 + \frac{Bn\left[1 - \exp\left(-m\left|\dot{\gamma}\right| \right) \right]}{\left|\dot{\gamma}\right|} \right) \dot{\gamma} \qquad (14)$$

Stream function equation:

$$\frac{\partial^2 \psi}{\partial x^2} + \frac{\partial^2 \psi}{\partial y^2} = \frac{\partial u}{\partial y} - \frac{\partial v}{\partial x} \qquad (15)$$

The boundary conditions relevant to the external walls and the interface of the flexible fin can be expressed as:

- On the left wall: (x = 0) : T = T_h, u = v = 0
- On the right wall: (x = H): T = T_c, u = v = 0
- On the top and the bottom: $\partial T/\partial n = 0$, u = v = 0
- On the interface of the flexible fin: $k_f \frac{\partial y}{\partial n}\Big|_f = k_s \frac{\partial y}{\partial n}\Big|_s$

2.2.2 Mathematical dimensionless equations

The governing dimensionless equations are obtained through the substitution of a set of dimensionless variables given by:

$$(U,V) = \frac{(u,v)L}{\alpha}, \quad \left(X,Y,D_s\right) = \frac{(x,y,d_s)}{L},$$

$$\tau = \frac{t\alpha}{L^2}, \; \theta = \frac{T - T_c}{T_h - T_c}, \; P = \frac{pL^2}{\rho\alpha^2},$$

$$\sigma^* = \frac{\sigma}{E}$$

The governing dimensionless equations are hence

Masse balance

$$\frac{\partial U}{\partial X} + \frac{\partial V}{\partial Y} = 0 \qquad (16)$$

Momentum balance:

$$\frac{\partial U}{\partial \tau} + U\frac{\partial U}{\partial X} + V\frac{\partial U}{\partial Y} = -\frac{\partial P}{\partial X} + \left(\frac{\partial \tau_{XX}^*}{\partial X} + \frac{\partial \tau_{XY}^*}{\partial Y} \right) \qquad (17)$$

$$\frac{\partial V}{\partial \tau} + U\frac{\partial V}{\partial X} + V\frac{\partial V}{\partial Y} = -\frac{\partial P}{\partial Y} + \left(\frac{\partial \tau_{XY}^*}{\partial X} + \frac{\partial \tau_{YY}^*}{\partial Y} \right) + Ra\,\mathrm{Pr}\,\theta \qquad (18)$$

The energy equation for the fluid:

$$\frac{\partial \theta}{\partial \tau} + U\frac{\partial \theta}{\partial X} + V\frac{\partial \theta}{\partial Y} = \frac{\partial^2 \theta}{\partial X^2} + \frac{\partial^2 \theta}{\partial Y^2} \qquad (19)$$

Structural displacement of the flexible fin:

$$\rho_R \frac{\partial^2 D_{sX}}{\partial \tau^2} - E_t\left(\frac{\partial \sigma_{XX}^*}{\partial X} + \frac{\partial \sigma_{XY}^*}{\partial Y} \right) = E_t F_{VX} \qquad (20)$$

$$\rho_R \frac{\partial^2 D_{sY}}{\partial \tau^2} - E_t\left(\frac{\partial \sigma_{XY}^*}{\partial X} + \frac{\partial \sigma_{YY}^*}{\partial Y} \right) = E_t F_{VY} \qquad (21)$$

D_s dimensionless displacement vector

The energy equation for the fin:

$$\frac{\partial \theta_s}{\partial \tau} = K_R\left(\frac{\partial^2 \theta_s}{\partial X^2} + \frac{\partial^2 \theta_s}{\partial Y^2} \right) \qquad (22)$$

Where ρ_R is the ratio of fluid to solid-structure density, and K_R he ratio of the thermal conductivity of the fluid to that of the solid structure

$$\rho_R = \frac{\rho_s}{\rho_f} \qquad K_R = \frac{k_s}{k_f} \qquad F_v = \frac{(\rho_f - \rho_s)L^* g}{E}$$

The Rayleigh and Prandtl numbers, as well as the Elasticity modulus, are introduced as :

$$Ra = \frac{\rho_f^2 c_p g \beta \Delta T L^2}{\mu_B k_f} \tag{23}$$

$$\Pr = \frac{c_p \mu_B}{k} \tag{24}$$

$$E_t = \frac{E \cdot L^{*2}}{\rho_f \alpha_f^{\,2}} \tag{25}$$

The Bingham number is defined as:

$$Bn = \frac{\tau_0 L^2}{\alpha \mu_B} \tag{26}$$

Consequently, the dimensionless viscosity η can be written as follows:

$$\eta = \frac{\mu_B}{\mu_P} = \left(1 + \frac{Bn\left[1 - \exp\left(-m\left|\dot{\gamma}\right|\right)\right]}{\left|\dot{\gamma}\right|} \right) \dot{\gamma} \tag{27}$$

Stream function equation:

$$\frac{\partial^2 \Psi}{\partial X^2} + \frac{\partial^2 \Psi}{\partial Y^2} = \frac{\partial U}{\partial Y} - \frac{\partial V}{\partial X} \tag{28}$$

The dimensionless initial boundary conditions are given as follows

- On the left wall: (X = 0) : θ = 1, U = V = 0
- On the right wall: (X = 1): θ = 0, U = V = 0
- On the top and the bottom: $\partial\theta/\partial N$ = 0, U = V = 0
- On the interface of the flexible fin: $k_r \left.\frac{\partial \theta}{\partial N}\right|_f = k_r \left.\frac{\partial \theta_s}{\partial N}\right|_s$

The non-dimensional heat transfer rates through the fluid in contact with the hot wall and the flexible fin are, respectively:

$$Nu_f = -\frac{k}{T_h - T_c}\frac{\partial \theta}{\partial X} \tag{29}$$

$$Nu_s = -k_r \frac{\partial \theta}{\partial X} \tag{30}$$

The average Nusselt number at the hot wall is also introduced as:

$$\overline{Nu} = \int_0^{s_1} Nu_f dy + \int_{s_1}^{s_2} Nu_s dy + \int_{s_2}^{1} Nu_f dy \Bigg| \begin{matrix} s_1 = \frac{1}{2} - \frac{t_{fin}}{2} \\ s_2 = \frac{1}{2} + \frac{t_{fin}}{2} \end{matrix} \tag{31}$$

3. Numerical method, grid study, and Code validation

3.1 Numerical solution method:

Numerical solution methods are employed to solve the governing equations and boundary conditions for the unsteady natural convection flow of a Bingham fluid inside a 2D square cavity with an elastic flexible fin. The equations are first transformed into a more manageable form and then solved using the Galerkin Method of Weighted Residuals, which is a type of the Finite Element Method (FEM). An Arbitrary Lagrangian-Eulerian (ALE) method is used to represent the fluid-structure interface and accurately capture the motion of the elastic fin. The computational domain is discretized into triangular, non-uniform elements, allowing for an accurate representation of the flow field. To handle the nonlinearity of the momentum equations, a Newton iteration algorithm is employed. The resulting numerical solution provides valuable insights into the behavior of Bingham fluids under natural convection and the potential for using flexible fins to enhance heat transfer in a range of engineering applications

3.2 Grid independency check:

In the field of numerical methods for solving physical problems, grid-independence tests are conducted to ensure that the results remain unaffected by the number of mesh elements employed. Within this context, we examine the average Nusselt number on the hot wall at Ra=10^5, Et=10^{10}, and Pr=10 for five different mesh sizes, as outlined in Table 1. The table presents the number of elements used in

the fluid domain and the corresponding Nusselt number for various mesh sizes in the steady state. It can be inferred that the grid with 82,933 elements (case 4) is suitable for all computations conducted in this paper.

Table 1: grid testing for Nuavg, Ψmax for different grid sizes for Et = 5×10^{10}, Ra = 10^5, Bn = 5

Grid size	Number of éléments	Time [s]	Ψmax	Nu avg
Case 1	21013	254	3.12549	1.73105
Case 2	37143	437	3.13121	1.73237
Case 3	57890	709	3.13558	1.73349
Case 4	82933	1225	3.13798	1.73443
Case 5	97262	1247	3.13897	1.73471

3.3 Code validation

In any numerical study, a crucial step is to verify the accuracy and validity of the presented results. Firstly, the isotherm contours obtained by Mohammad Shahabadi et al for the Prandtl number (Pr) = 10 and the Eckert number (Et) = 10^{10} have been employed to validate the findings of the current study. As depicted in Figure 2, the numerical results from this study exhibit a close agreement with Shahabadi's literature. To further verify the numerical method and obtained results, the Nusselt number is calculated for different Rayleigh numbers and compared with those of Shahabadi et al [5]. As displayed in Table 2, the maximum difference between the current results and those obtained by Shahabadi et al [5] is 3.474%. These comparisons confirm the accuracy and precision of the numerical method used in the current study. Although full analyses of the findings are provided in the original paper [5]

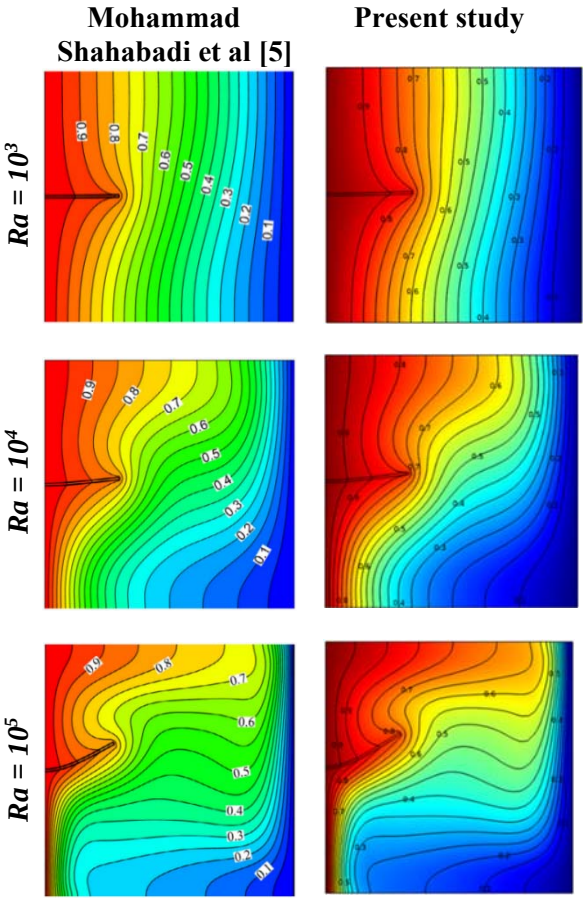

Fig . 2 Comparison of isotherms between Mohammad Shahabadi et al [5] and the current study for different values of Ra when n = 1, Et =10^{10} ,Pr=10

Table 2 The average Nusselt (Nu) for different Rayleigh number at Pr =10

	Nu_{avg}		
	Mohammad Shahabadi et al [5]	Présent study	Error %
$Ra = 10^3$	1.08949	1.12423	3.474
$Ra = 10^4$	1.93385	1.92136	1.249
$Ra = 10^5$	4.41245	4.41572	0.327

4. Results and discussion

In this section, we analyze in detail the influence of various parameters on thermos-fluid flow and deformation phenomena within the flexible fin. Parameters intentionally varied include the modulus of elasticity, ranging from 5×10^{10} to 5×10^{11}, the Rayleigh number, spanning from 10^3 to 10^5, elastic fin length (Lc 0.004-0.0073), Prandtl number (Pr 0.71-100), and the variation of the Bingham number from 0 to 20.

It should be noted that certain key parameters, such as the dimensionless body force (maintained at a constant value of Fv=0)the fixed thermal conductivity ratio (k_R=100), as well as the constant density ratio (ρ_R=1), are held steady throughout the numerical simulations. This is done with the aim of isolating the specific influence of the aforementioned variable parameters. The results of these investigations are presented in the form of isothermal contours and vortex structures, accompanied by detailed graphs representing Nusselt numbers and observed deformations. This presentation provides an in-depth understanding of the phenomena under study.

4.1 Time variation study

Figures 3 and 4 show the progression of the isotherms and streamlines over time for Ra = 10^5, Et = 5×10^{10}, Bn = 0, and Pr = 10. At the initial stage (τ = 10), the flexible elastic fin is stationary because conduction is the dominant mode of heat transfer. At a later stage (τ = 50), fluid motion increases, leading to enhanced heat transfer and the movement of the flexible fin towards the top of the hot wall.

As time progresses, between $100 \leq \tau \leq 300$, more disturbances and vortices can be observed around the fin, and the isotherms become more deviated, indicating that convection is becoming more significant along with conduction. In the steady state (τ = 2000), the flexible fin experiences its maximum shift and fluid flow circulation.

According to Figure 4, at the initial time step, two vortices appear, one of a small size on the vertical hot wall and the other much larger next to the cold wall, due to low heat transfer by convection. As time passes, the number of vortices decreases, with only one vortex remaining next to the cold wall. In the steady state, there is always one weak vortex present next to the cold wall.

Figure 5 illustrates the correlation between the Nusselt number and the Bingham number under the conditions Ra = 105, Et = 5 × 1010, and Pr = 10 on the hot wall over time. In the initial stage (0 to 10), the impact of the Bingham number on the Nusselt number is limited because conduction is the dominant mode of heat transfer. As time progresses, the influence of the Bingham number on the

average Nusselt number becomes more significant. It is noteworthy that when the fluid is classified as Newtonian (Bn = 0), heat transfer is higher, resulting in a higher Nusselt number. Conversely, the average Nusselt number decreases as the Bingham number increases. This is due to the fact that increasing the Bingham number makes the fluid more non-Newtonian, leading to an increase in viscosity with shear rate, hindering the fluid's ability to flow, and slowing its flow rate.

Figure 6 shows the variation of maximum stress as a function of time for various Bingham numbers at Et = 5 × 1010, Pr = 10, and Ra = 105. As observed, the variation in the Bingham number has a significant effect on the maximum stress and fin deformation. It is remarkable that an increase in the Bingham number leads to an increase in fin deformation, reaching its maximum at Bn = 20. This is because an increase in the Bingham number causes a blockage of the flow, resulting in an increase in the friction coefficient and, consequently, an increase in the fin deformation level.

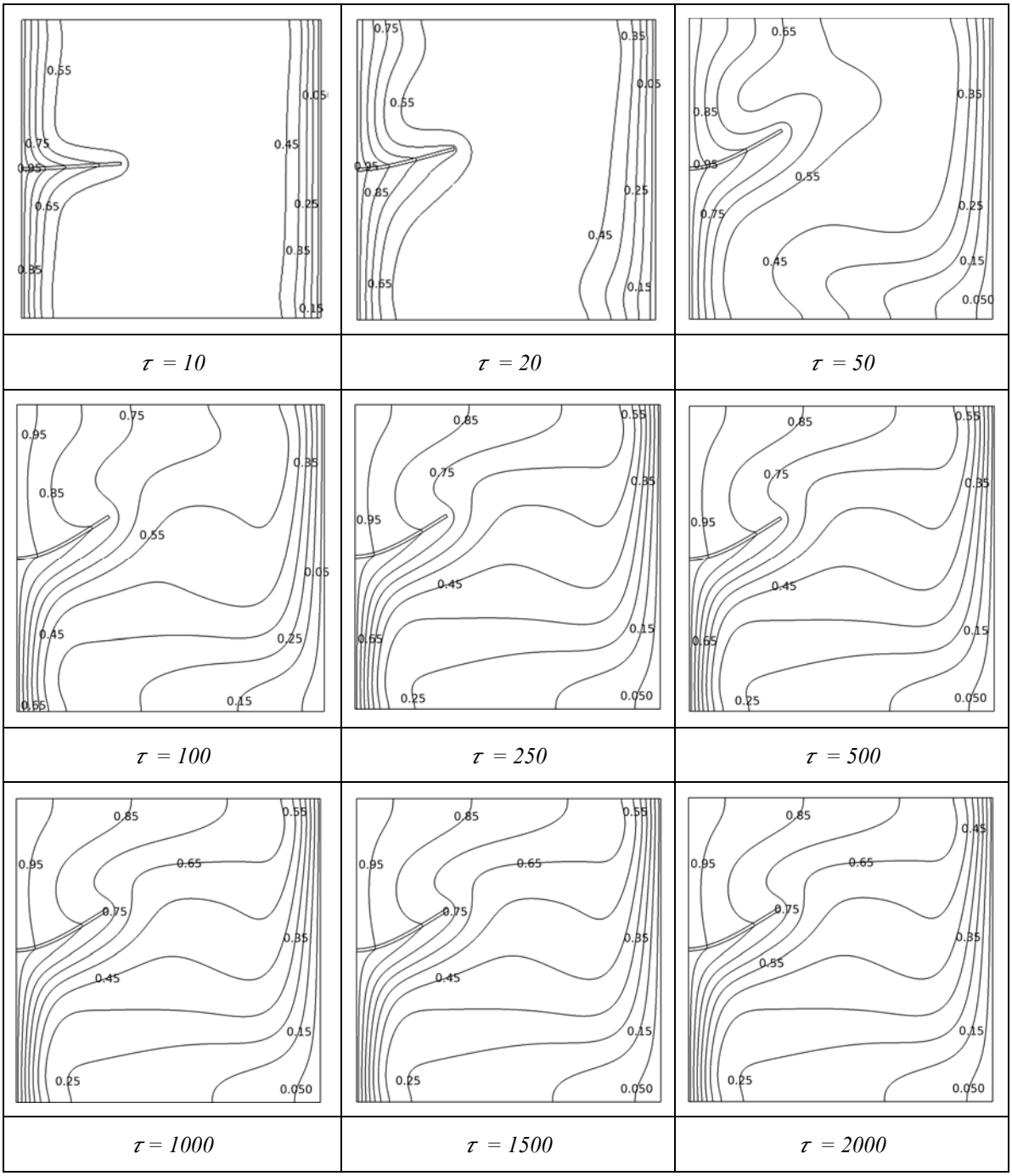

Fig 3: Development of isotherms and the deformation of the flexible fin with time at $Ra = 10^5$, $Pr = 10$, $Bn = 0$ and $Et = 5\times10^{10}$

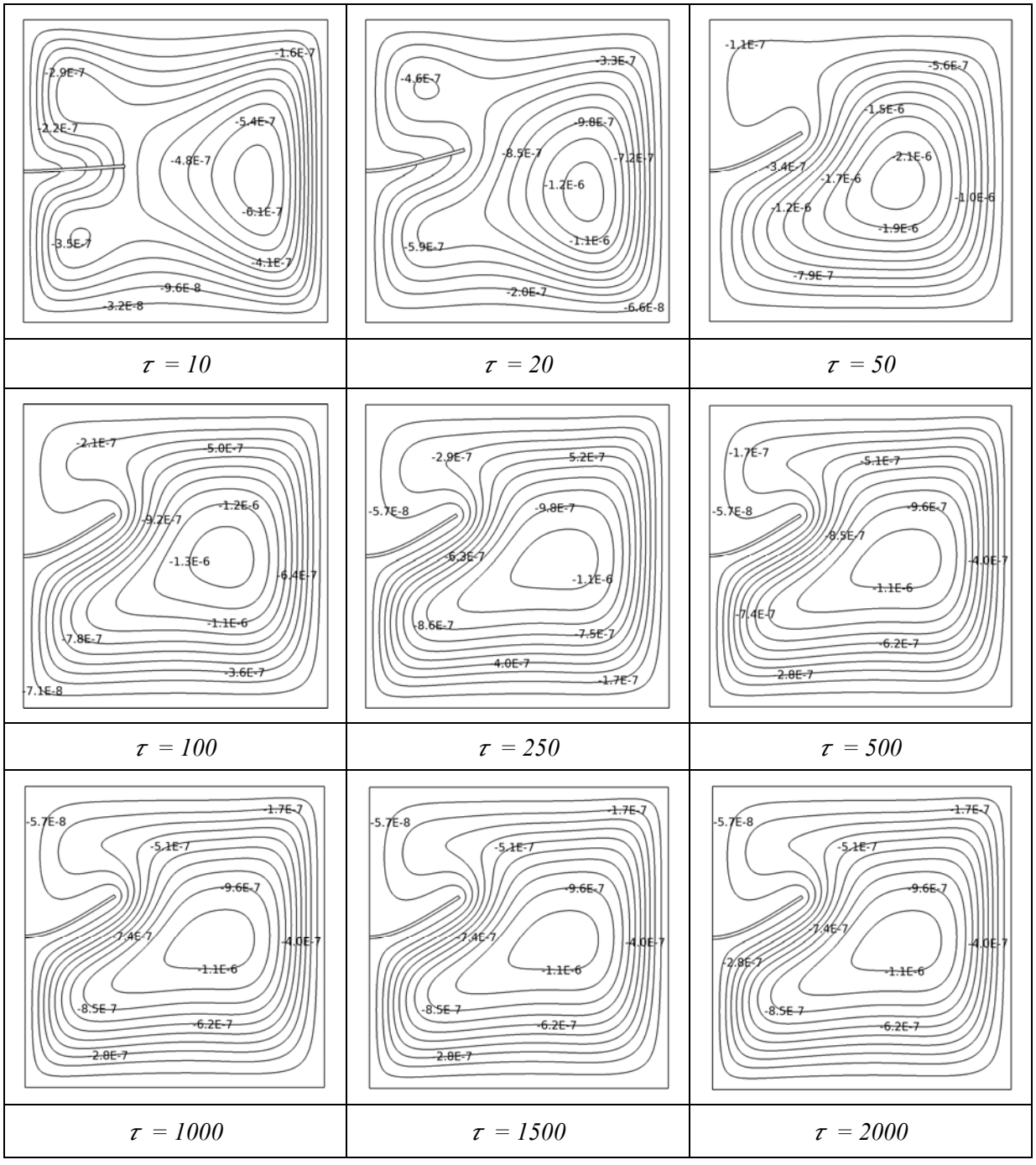

Fig . 4. Development of streamline with time at $Ra = 10^5$, $Pr = 10$, $Bn = 0$ and $Et = 5\times10^{10}$

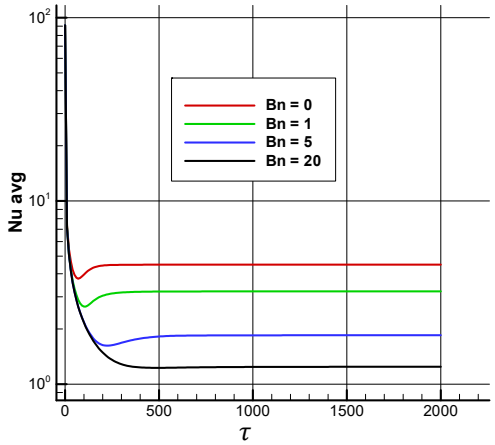

Fig . 5. The variation of Nusselt number along the hot wall with time for different Bingham number at Et=5×10^{10} Ra = 10^{5} and Pr=10

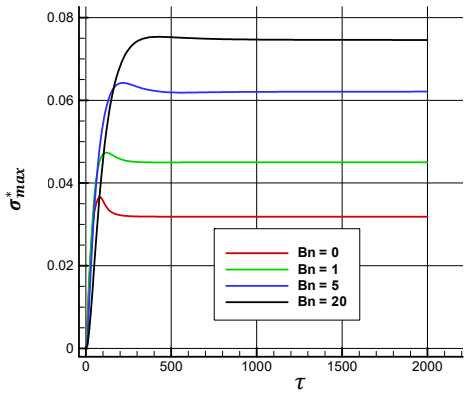

Fig . 6. The variation of the values of maximum stress with time for different Bingham number at Et=5×10^{10} Ra = 10^{5} and Pr=10

4.2 The effects of elasticity modulus:

Figure 7 demonstrates the impact of different values of the elasticity modulus (Et) on isotherm contours with varying Bingham numbers. It can be observed that at a lower elasticity modulus (Et = 5 × 10^{10}), the flexible fin bends more easily, and the deformation increases with an increasing Bingham number, reaching the greatest deformation at Bn = 20. Conversely, as the elasticity modulus increases, the resistance of the flexible fin also increases, resulting in a decrease in its displacement.

Figure 8 examines the influence of the modulus of elasticity and Bingham number on vortex formation in fluid flow. In a Newtonian fluid (Bn = 0), a single large vortex is observed near the left wall, decreasing in size as the modulus of elasticity increases. On the other hand, an increase in the Bingham number and the yield stress causes a reduction in the size of the vortex. This reduction is due to the increasingly non-Newtonian behavior of the fluid as the Bingham number increases, leading to an increase in viscosity as a function of shear rate. This increased viscosity makes it more difficult for the fluid to flow, and once the fluid starts to flow, its rate of flow is slower than that of a Newtonian fluid with the same viscosity. As a result, the number of vortices in the flow decreases, leaving only a small vortex near the cold wall. This vortex decreases in intensity as the Bingham number increases (1 ⩽ Bn ⩽ 20).

As the Bingham number increases, this phenomenon can be interpreted as a transition from convection to conduction in heat transfer.

Figure 9 presents the variation of the average Nusselt number on the hot wall for different values of the elasticity modulus at Ra = 105 and Pr = 10. It can be observed that the average Nusselt number decreases as the elasticity modulus reduces. Overall, the elasticity modulus has a negligible effect on the average Nusselt number. The higher average Nusselt number is observed in the steady state for the higher elasticity modulus (Et = 5 × 1011).

Figure 10 illustrates the variation of the maximum stress as a function of the Bingham number for different moduli of elasticity at Ra = 105 and Pr = 10.

It is noticeable that the maximum stress and deformation of the fin decrease with the increase in the modulus of elasticity. This is due to the increased resistance of the fin to deformation, leading to a drop in the deformation. The maximum value of the deformation is noted for Et = 5 × 1010 at Bn = 20.

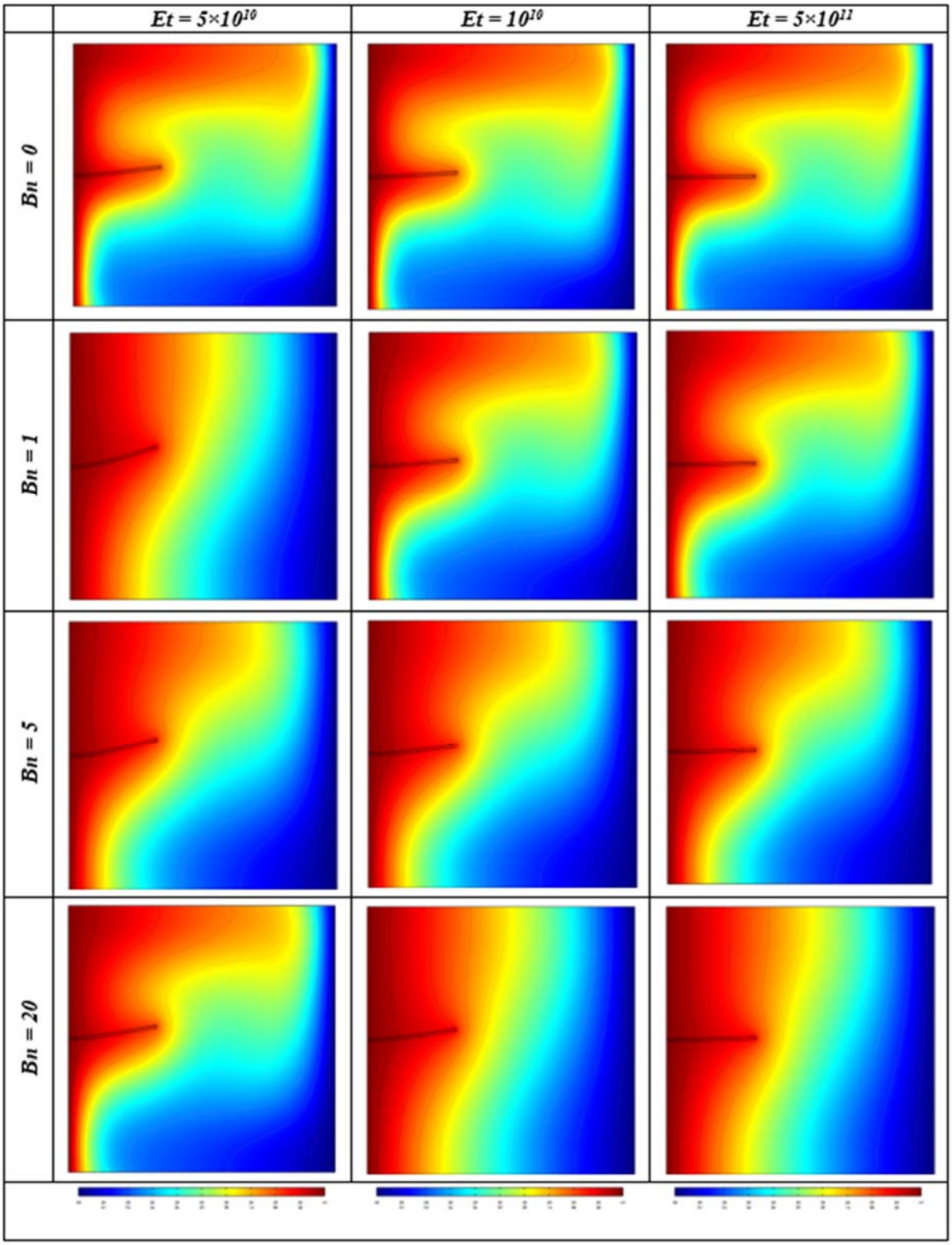

Fig. 7. Isotherms contours for different values of elasticity modulus (Et) and various Bingham number (Bn) at Pr = 10 at Ra = 10^5

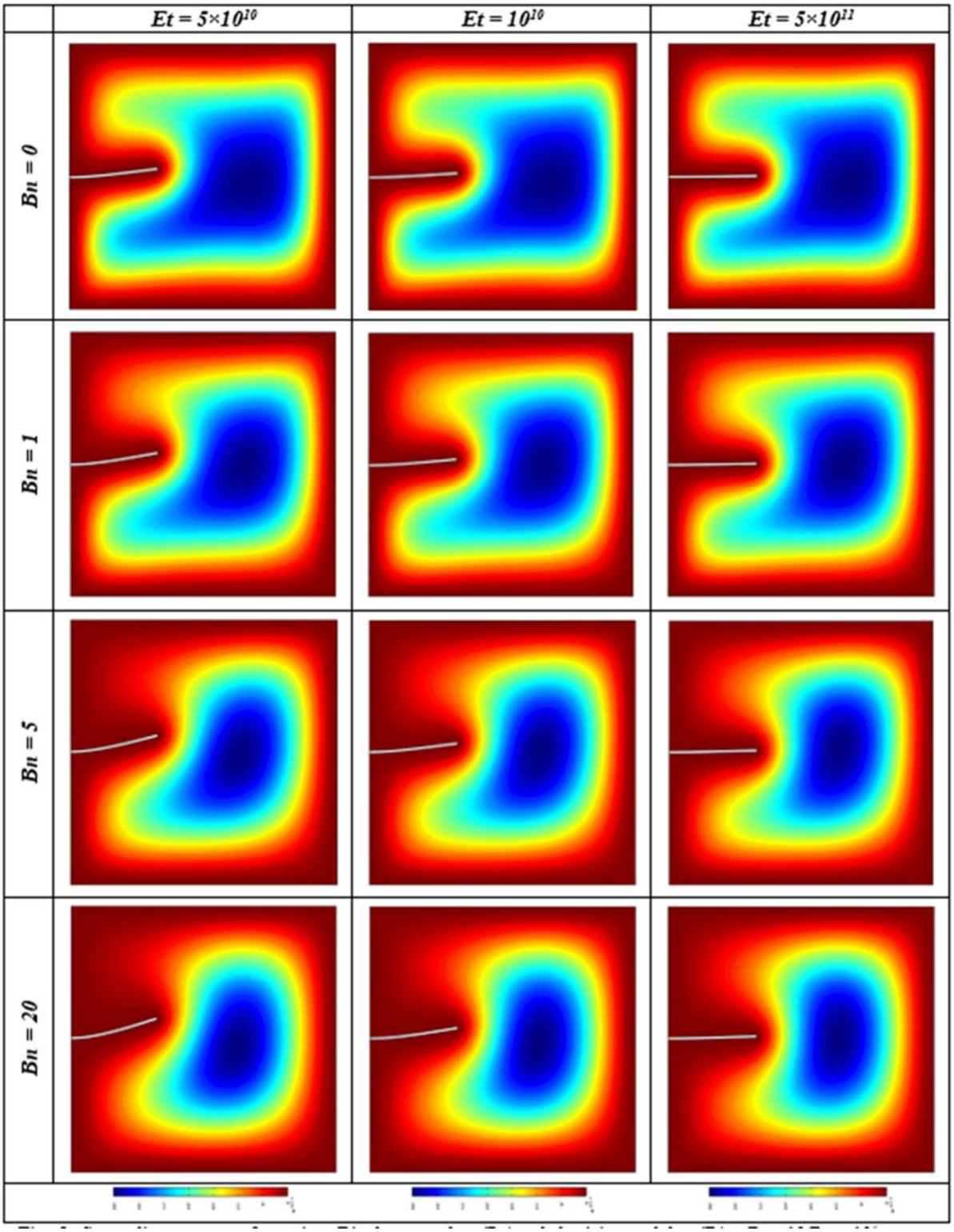

Fig. 8. Streamlines contours for various Bingham number *(Bn)* and elasticity modulus *(Et)* at P r= 10,Ra = 10^5

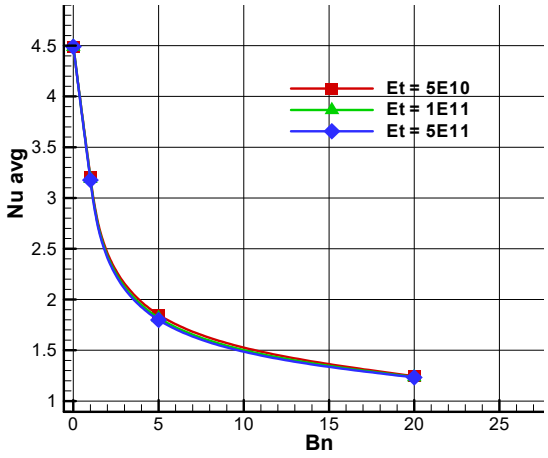

Fig. 9. The variation of Nusselt number along the hot wall for different Elasticity modulus at Ra=10^5 and Pr=10

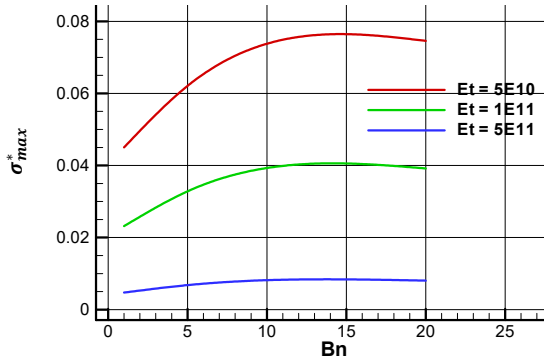

Fig. 10. The variation of the values of maximum stress for different Elasticity modulus at Ra=10^5 and Pr=10

4.3 The effects of Rayleigh number:

The impact of varying the Rayleigh number for different values of the Bingham number on the isotherms and streamline contours at Et = 5×10^{10} and Pr = 10 is illustrated in Figures 11 and 12. As observed, for a low Rayleigh number (Ra = 10^3), the flexible fin remains stationary, and the transfer is supposed to be by conduction only. Increasing the Rayleigh number (Ra = 10^4) causes an increase in fluid circulation and fin motion, with natural convection becoming more intense. At a higher Rayleigh number (Ra = 10^5), natural convection becomes the main heat transfer mechanism, and it can be seen that the fin reaches its maximum displacement for Et = 5×10^{10} and Bn = 20.

According to Figure 12, for low Rayleigh numbers (Ra = 10^3), it is possible to notice the presence of a single vortex in the center of the cavity of the same size for different Bingham numbers, and the streamlines are symmetrical with respect to the horizontal axis. This indicates that conduction is the main mechanism of heat transfer. At Rayleigh number (Ra = 10^4), the vortices become more important when the fluid is considered Newtonian (Bn = 0). Then, for a higher Rayleigh number (Ra = 10^5), the vortex

formed in the center of the cavity moves near the cold wall, and it always remains much more important for the Newtonian case. The pattern of the streamlines indicates that natural convection is the main mechanism of heat transfer.

Figure 13 shows the impact of the Rayleigh number on the average Nusselt for various Bingham numbers at Et = 5×10^{10} and Pr = 10. It has been observed that the average Nusselt number for (Ra = 10^5) is higher than other Rayleigh numbers (Ra = 104) and (Ra = 10^3), respectively. It is interesting to note that the average Nusselt number increases as the Rayleigh number increases. It is essential to note that the average Nusselt decreases with an expanding Bingham number until it achieves a steady incentive for a high Bingham number (Bn = 20), showing that the intensity of the heat transfer is exclusively through conduction.

Figure 14 illustrates the variation of the maximum stress as a function of the Bingham number for different Rayleigh numbers at Pr = 10 and Et = 5×10^{10}. For Ra = 10^3, the deformation of the fin is negligible. With increasing buoyancy forces (Ra = 10^4), the deformation increases until it reaches its maximum (Ra = 10^5). It is interesting to note that the deformation also increases with the increase in Bingham number. The maximum deformation is seen at the steady state for the higher Rayleigh number (Ra = 10^5) and Bingham number (Bn = 20)

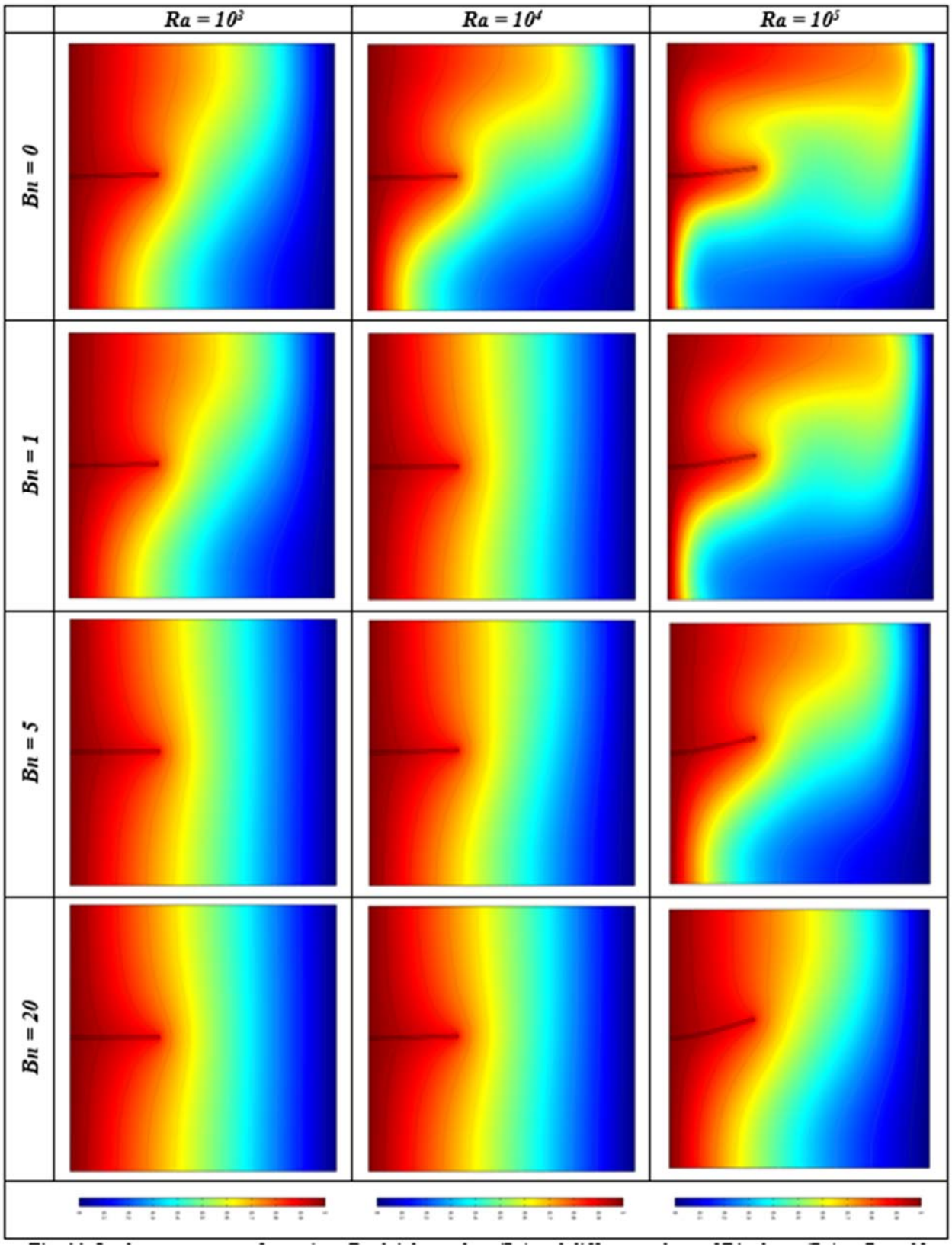

Fig. 11. Isotherms contours for various Rayleigh number *(Ra)* and different values of Bingham *(Bn)* at *Pr = 10* *Et* = 5×10^{10}.

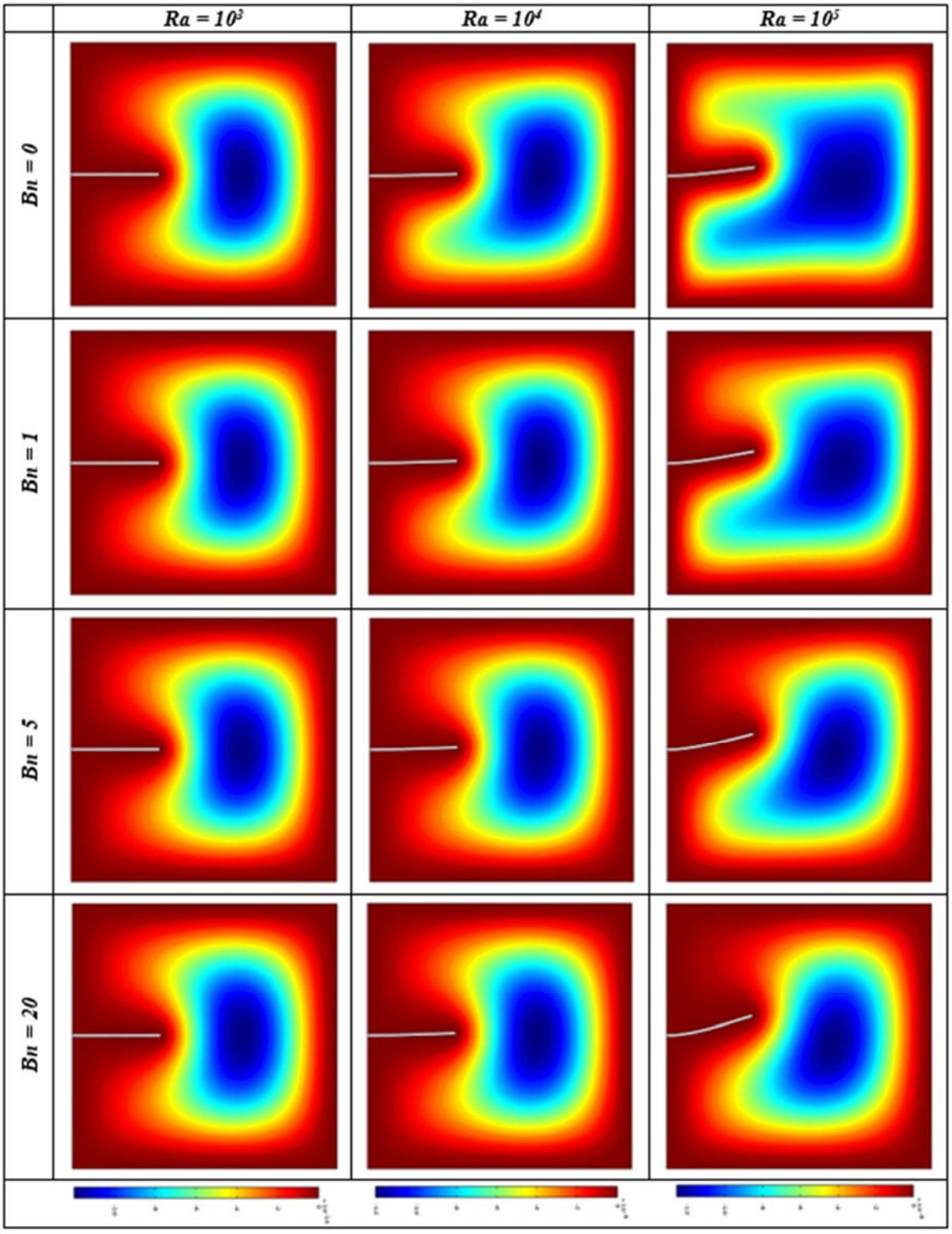

Fig. 12. Streamline contours for various Rayleigh number (Ra) and Bingham *(Bn) at Pr = 10, Et = 5×10^10*.

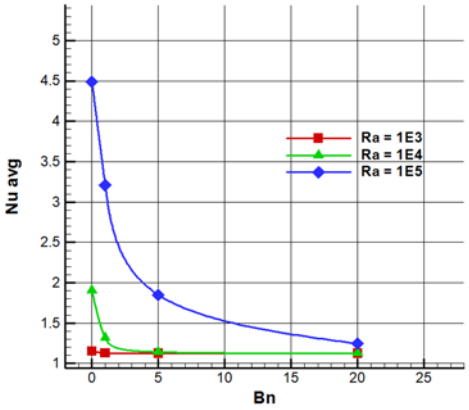

Fig. 13. The variation of Nusselt number along the hot wall for different Rayleigh number at Et=5×10^{10} and Pr=10

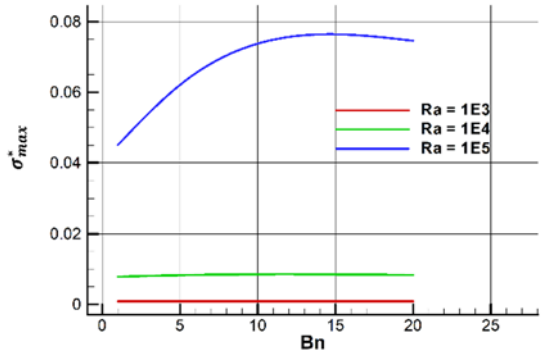

Fig. 14. The variation of maximum stress for different Rayleigh number at Et=5×10^{10} and Pr=10

4.4 The effects of Prandtl number:

Figure 15 displays the effects of the Prandtl number (Pr) and different values of the Rayleigh number (Ra) on the isotherms in a steady state at Bn = 5 and Et = 10^{11}. As previously defined, an increase in the Rayleigh number indicates an intensification of buoyancy forces in the fluid, resulting in a significantly greater deformation of the elastic fin. Additionally, the isothermal lines move toward the fin, indicating an increase in the rate of heat transfer. Furthermore, an increase in the Prandtl number implies an enhancement in the fluid's ability to transfer heat relative to its ability to move. It should be noted that maximum deformation is observed at high Prandtl values. This observation stems from the fact that momentum diffusion is more significant than heat diffusion when the Prandtl number is higher.

Figures 16 and 17 illustrate the impact of the Prandtl number on the average Nusselt number and the maximum stress for different values of the Rayleigh number, with Bn = 5 and Et = 1011. The increase in the Rayleigh number leads to heightened buoyancy forces, resulting in a significant improvement in the heat transfer rate. This improvement is particularly noticeable in the values of Nuavg (average Nusselt number) and σmax (maximum stress) for Ra = 105 compared to Ra = 104 and Ra = 103. Additionally, the increase in the Prandtl number favors improved heat transfer and a maximum increase in the deformation of the elastic fin, leading to higher values of Nuavg and , particularly for high values of Prandtl.

4.5 Effect of elastic fin length

Figure 18 shows the contours of the isotherms and streamlines for different lengths of the elastic fin, with Ra = 105, Bn = 5, Pr = 10, and Et = 5 × 1010. A significant observation was made: as the length of the elastic fin increases, so does the deformation, indicating a noticeable intensification of natural convection. It should be noted that this increase in deformation reaches a maximum peak at LC = 0.0073.

The effect of elastic fin length on the time variation of the average Nusselt number and maximum stress is depicted in Figures 19 and 20. It can be seen that, as the length of the elastic fin increases, the values of the average Nusselt number are reduced. This means that the overall rate of heat transfer is reduced as the length of the elastic fin increases. At the same time, an increase in fin deformation is observed as the fin length increases, as the stresses exerted on the fin increase in proportion to its increasing length.

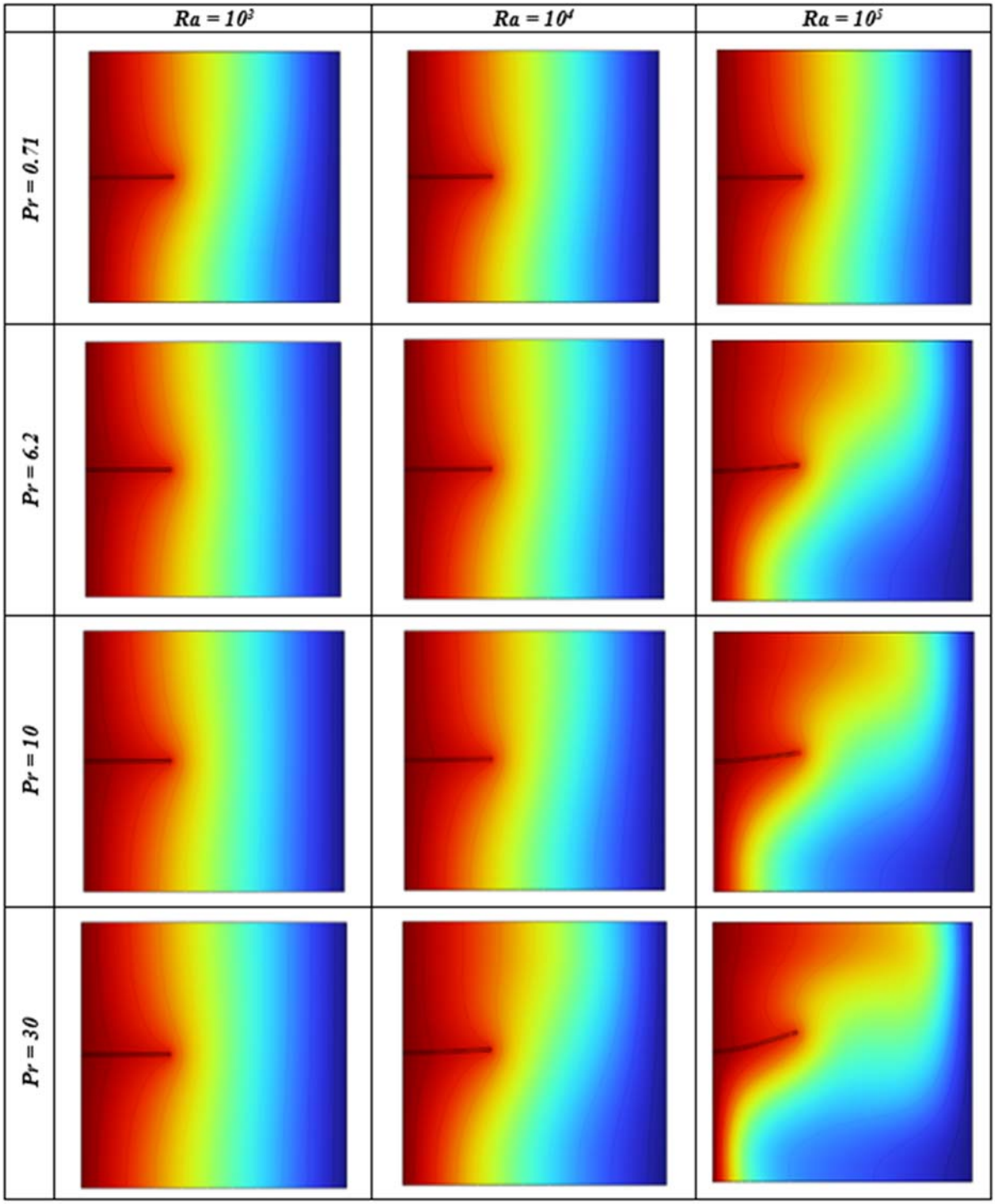
Ra = 10³
Ra = 10⁴
Ra = 10⁵
Pr = 0.71
Pr = 6.2
Pr = 10
Pr = 30

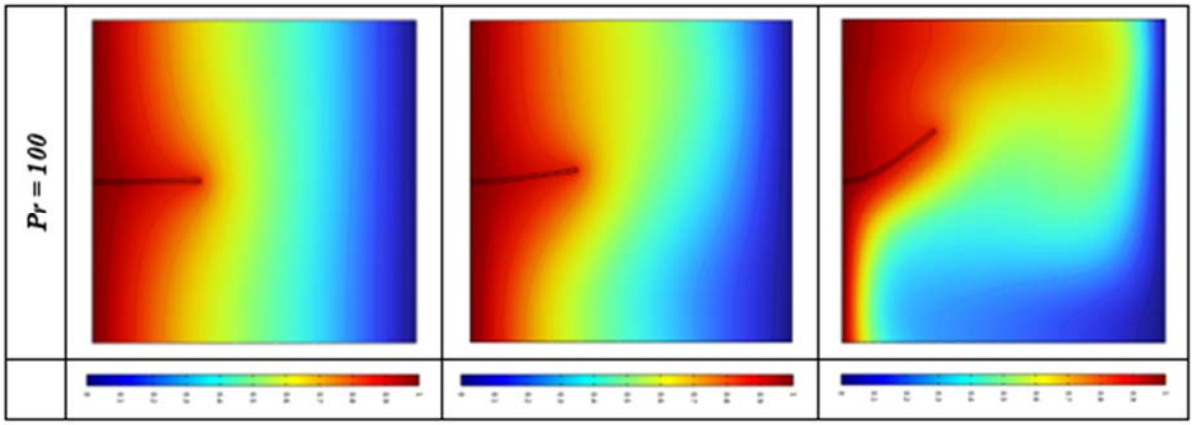

Fig. 15. Isotherms contours for various Prandtl number *(Pr)* and different values of Rayleigh (Ra) at *Bn = 5* and *Et=10^11*

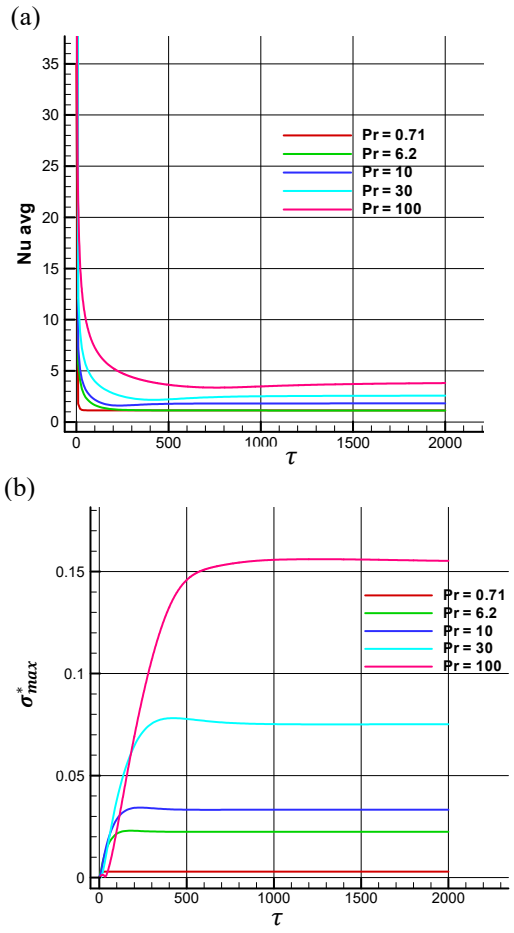

Fig. 16. The variation of Nusselt number *(a)* , maximum stress *(b)* for different Prandtl number *at Et=10^11* and *Bn=5 Ra= 10^5* over time

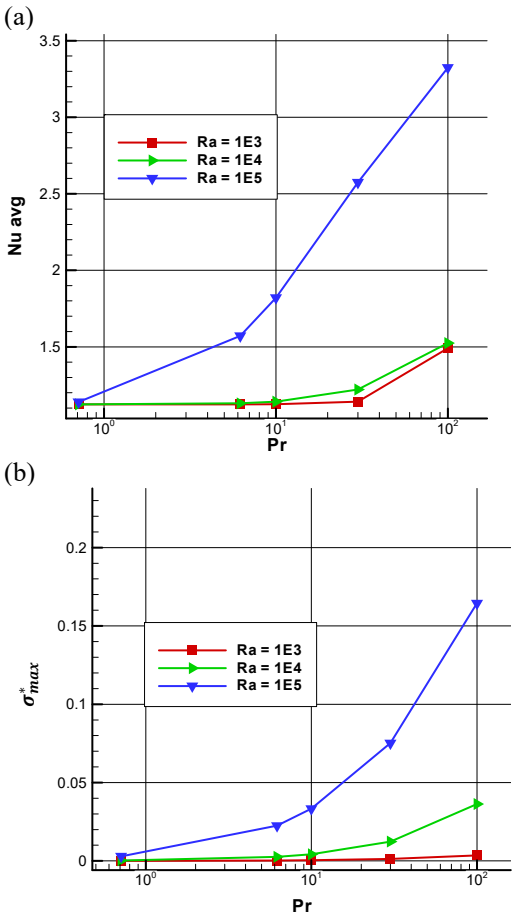

Fig. 17. The variation of Nusselt number *(a)*, maximum stress *(b)* for different Rayleigh number at *Et=10^11* and *Bn = 5*

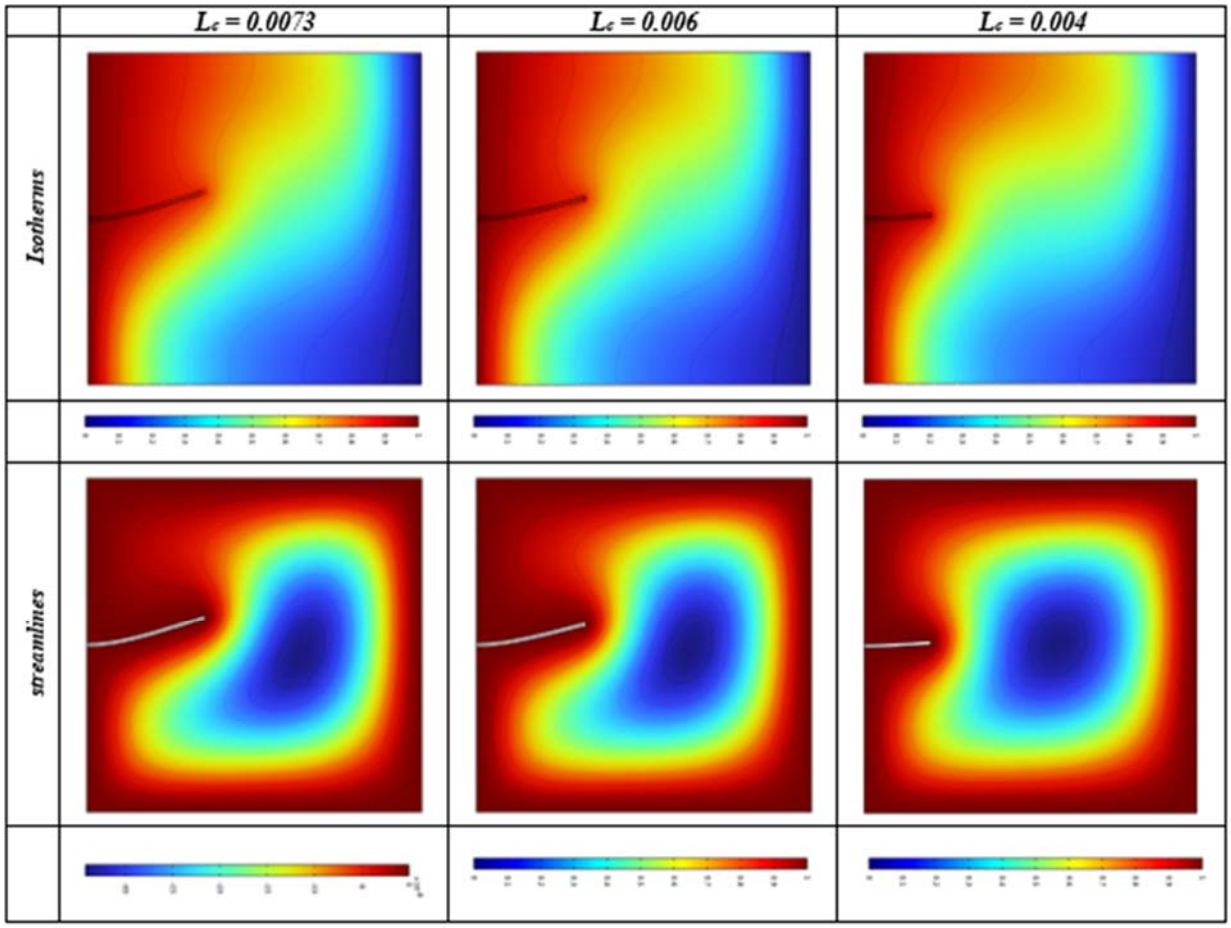

Fig. 18. Isotherms and streamlines contours for different values of L_C at Bn = 5 Ra= 10^5 and Et=5×10^{10}

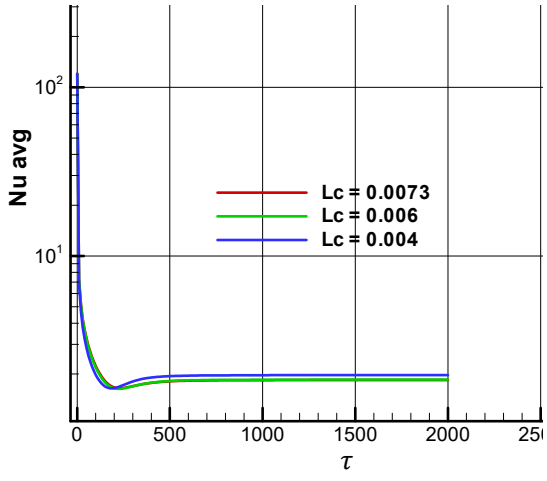

Fig. 19. The variation of Nusselt number along the hot wall for different elastic fin length at *Et* 5×10^{10}, *Pr = 10 , Ra =*$10^5$and *Bn=5* over time

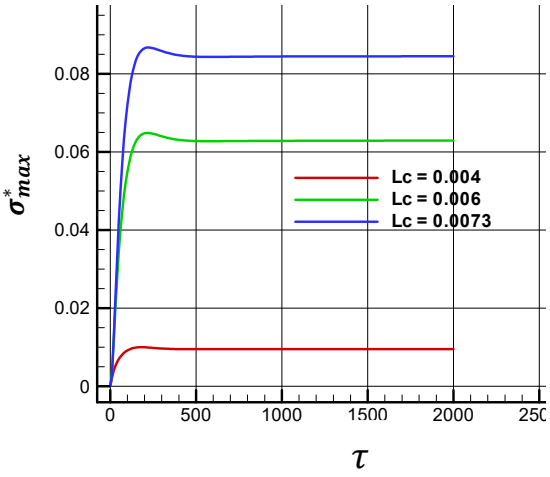

Fig. 20. The variation of maximum stress for different elastic fin length at *Et = 5×*10^{10}*, Pr = 10 , Ra =*$10^5$and *Bn =5* over time

5. Conclusion

Numerical investigations were carried out to explore the natural convective flow of a Bingham fluid within a square enclosure, utilizing the finite element method. The study focused on analyzing the effects of the Rayleigh number (Ra) and modulus of elasticity (Et), Bingham number (Bn) Prandtl number (Pr) on convective flow and heat transfer.

The main conclusions of this research can be succinctly stated as follows:

In the absence of a threshold constraint, when the fluid is considered Newtonian (Bn = 0), an increase in the Rayleigh number significantly impacts the improvement of the Nusselt number, reaching its optimum at Ra = 10^5. Particularly, the most pronounced deformation of the fin occurs when the elasticity modulus is moderate (Et = 5×10^{10}). However, it is important to note that the elasticity modulus has a negligible influence on heat transfer.

By increasing the Bingham number, the effect of the threshold constraint dominates in the flow, completely nullifying the buoyancy-induced flow until the Nusselt number reaches a constant value, corresponding to the conduction limit. In contrast, the deformation of the elastic fin gradually increases with an increase in the Bingham number, reaching its maximum for (Et = 5×10^{10}) and (Bn = 20).

The analysis of heat transfer reveals a positive correlation with the Rayleigh number and an inverse correlation with the Bingham number. Furthermore, increasing the fin's length has a positive impact on the deformation phenomenon while showing a slight influence on the heat transfer process. Finally, an increase in the Prandtl number effectively promotes heat transfer while inducing an increase in the deformation of the elastic fin.

Reference

[1] M. Ghalambaz, S.A.M Mehryan, A.I Alsabery, A. Hajjar, M. Izadi, A. Chamkha, Controlling the natural convection flow through a flexible baffle in an L-shaped enclosure, Meccanica, (2020) 1561-1584.

[2] M. Ghalambaz, S.A.M. Mehryan, R.K . Feeoj, A. Hajjar, I. Hashim, R. Babaei Mahani, Free convective heat transfer of a non-Newtonian fluid in a cavity containing a thin flexible heater plate: an Eulerian–Lagrangian approach, Journal of Thermal Analysis and Calorimetry, (2020) 1-6.

[3] E. Jamesahar, M. Ghalambaz, A.J . Chamkha, Fluid–solid interaction in natural convection heat transfer in a square cavity with a perfectly thermal-conductive flexible diagonal partition, International Journal of Heat and Mass Transfer, (2016) 303-319.

[4] S.A.M. Mehryan, A. Alsabery, A. Modir, E. Izadpanahi, M. Ghalambaz, Fluid-structure interaction of a hot flexible thin plate inside an enclosure, International Journal of Thermal Sciences, (2020) 106340.

[5] M. Shahabadi, S.A.M. Mehryan, M. Ghalambaz, M . Ismael, Controlling the natural convection of a non-Newtonian fluid using a flexible fin, Applied Mathematical Modelling. (2021) 669-686.

[6] S.M. Zadeh, S.A.M. Mehryan, E. Izadpanahi, M. Ghalambaz, Impacts of the flexibility of a thin heater plate on the natural convection heat transfer, International Journal of Thermal Sciences, (2019) 106001.

[7] A . Raisi, I . Arvin , A numerical study of the effect of fluid-structure interaction on transient natural convection in an air-filled square cavity, International Journal of Thermal Sciences, (2018) 1-4.

[8] A.I .Alsabery, M.A. Sheremet, M . Ghalambaz, A.J. Chamkha, I. Hashim, Fluid-structure interaction in natural convection heat transfer in an oblique cavity with a flexible oscillating fin and partial heating, Applied Thermal Engineering, (2018) 80-97.

[9] K. Khanafer, K. Vafai, Effect of a circular cylinder and flexible wall on natural convective heat transfer characteristics in a cavity filled with a porous medium, Applied Thermal Engineering, (2020) 115989.

[10] H. Saleh, I. Hashim, E. Jamesahar, M. Ghalambaz, Effects of flexible fin on natural convection in enclosure partially-

filled with porous medium ☆ , Alexandria Engineering Journal (2020) 3515-3529.

[11] A. Dutta, A.K. Gupta, G. Mishra, R.P. Chhabra RP, Effect of fluid yield stress and of angle of tilt on natural convection from a square bar in a square annulus, Computers & Fluids. (2018) 138-163.

[12] M. Ghalambaz, E. Jamesahar, M.A. Ismael, A.J. Chamkha, Fluid-structure interaction study of natural convection heat transfer over a flexible oscillating fin in a square cavity, International Journal of Thermal Sciences, (2017) 256-273.

[13] H. Saleh, K. Naganthran, I. Hashim, M. Ghalambaz, R. Nazar, Role of fluid-structure interaction in free convection in square open cavity with double flexible oscillating fins, Alexandria Engineering Journal, (2022) 1217-1234.

[14] S.A. Mehryan, M. Ghalambaz, M.A. Ismael, A.J. Chamkha, Analysis of fluid-solid interaction in MHD natural convection in a square cavity equally partitioned by a vertical flexible membrane, Journal of Magnetism and Magnetic Materials, (2017) 161-173.

[15] M. Sairamu, R.P. Chhabra RP, Natural convection in power-law fluids from a tilted square in an enclosure, International Journal of Heat and Mass Transfer, (2013) 319-339.

[16] A.B. Shahrestani, B. Alshuraiaan, M. Izadi, Combined natural convection-FSI inside a circular enclosure divided by a movable barrier, International Communications in Heat and Mass Transfer, (2021) 105426.

[17] A.M. Aly, Z.A. Raizah, Coupled fluid-structure interactions of natural convection in a ferrofluid using ISPH method, Alexandria Engineering Journal, (2019) 1499-1516.

[18] T. Long, C. Huang, D. Hu, M. Liu, Coupling edge-based smoothed finite element method with smoothed particle hydrodynamics for fluid structure interaction problems, Ocean Engineering, (2021) 108772.

[19] P. Yang, C. Huang, Z. Zhang, T. Long, M. Liu, Simulating natural convection with high rayleigh numbers using the smoothed particle hydrodynamics method, International Journal of Heat and Mass Transfer, (2021) 120758.

[20] N. Nirmalkar, A. Bose, R.P. Chhabra, Free convection from a heated circular cylinder in Bingham plastic fluids, International journal of thermal sciences, (2014) 33-44.

[21] M. Sairamu, N. Nirmalkar, R.P. Chhabra, Natural convection from a circular cylinder in confined Bingham plastic fluids, International Journal of Heat and Mass Transfer (2013) 567-581.

[22] S. Yigit, R. Poole, Chakraborty, Effects of aspect ratio on natural convection of Bingham fluids in rectangular enclosures with differentially heated horizontal walls heated from below, International Journal of Heat and Mass Transfer, (2015) 727-736.

[23] S. Yigit, Chakraborty, Laminar natural convection of Bingham fluids in square cross-sectioned cylindrical annular cavity with differentially heated vertical walls subjected to constant heat fluxes, Heat Transfer Engineering, (2017) 1171-1188

[24] S. Yigit, S. Chen, P. Quinn, Chakraborty, Numerical investigation of laminar Rayleigh-Bénard convection of Bingham fluids in square cross-sectioned cylindrical enclosures, International Journal of Thermal Sciences, (2016) 356-368.

[25] O. Turan, S. Yigit, Chakraborty, Critical condition for Rayleigh-Bénard convection of Bingham fluids in rectangular enclosures, International Communications in Heat and Mass Transfer, (2017) 117-125.

[26] S. Yigit, T. Foxon, Chakraborty, Influences of boundary condition on laminar natural convection of Bingham fluids in square cross-sectioned cylindrical annular enclosures with differentially heated vertical walls, Heat Transfer Engineering, (2018) 319-338.

[27] G.R. Kefayati, H. Tang, A. Chan, Immersed Boundary-Finite Difference Lattice Boltzmann method through fluid–structure interaction for viscoplastic fluids, Journal of Fluids and Structures, (2018) 238-258.

[28] M.K. Nayak, N. Karimi, A.J. Chamkha, A.S. Dogonchi, S. El-Sapa, A.M. Galal,

Efficacy of diverse structures of wavy baffles on heat transfer amplification of double-diffusive natural convection inside a C-shaped enclosure filled with hybrid nanofluid, Sustainable Energy Technologies and Assessments, (2022) 102180.

[29] P.K. Das, A.K. Gupta, N. Nirmalkar, R.P. Chhabra, Effect of confinement on forced convection from a heated sphere in Bingham plastic fluids, Korea-Australia Rheology Journal, (2015) 75-94.

[30] H.A. Jahromi, A. Raisi, B. Ghasemi, A.A. Nadooshan, Numerical study of the Bingham fluid flow in a cylindrical enclosure with exact Bingham model, Journal of the Brazilian Society of Mechanical Sciences and Engineering, (2020) 162.

[31] A.K. Gupta, S. Gupta, R.P. Chhabra, Natural convection in Bingham plastic fluids from an isothermal spheroid: Effects of fluid yield stress, viscous dissipation and temperature-dependent viscosity, Korea-Australia Rheology Journal, (2017) 163-184.

[32] T.S. Devi, C.V. Lakshmi, K. Venkatadri, M.S. Reddy, Influence of external magnetic wire on natural convection of non-Newtonian fluid in a square cavity, Partial Differential Equations in Applied Mathematics, (2021) 100041.

[33] N. Labsi, Y.K. Benkahla, A. Boutra, M. Titouah, Convection heat transfer inside a lid-driven cavity filled with a shear-thinning Herschel–Bulkley fluid, Journal of the Brazilian Society of Mechanical Sciences and Engineering, (2018) 1-25.

[34] O.M. Lavrenteva, Y. Holenberg, A. Nir, Marangoni and natural convection in a horizontal layer of viscoplastic fluid with concentration dependent yield stress, Exact analytical solutions. Microgravity Science and Technology, (2009) 59-65.

[35] Z. Youbi, B. Benaouda-Zouaoui, C. Nouar, Study of cooling with solidification of a laminar thermodependent Herschel-Bulkley fluid flow in a convectively cooled annular duct, Acta mechanica, (2001) 15-29.

[36] W.A. Sabbar, M.A. Ismael, M. Almudhaffar, Fluid-structure interaction of mixed convection in a cavity-channel assembly of flexible wall, International Journal of Mechanical Sciences, (2018) 73-83.

[37] M.A. Ismael, H.F. Jasim, Role of the fluid-structure interaction in mixed convection in a vented cavity, International Journal of Mechanical Sciences. (2018) 190-202.

[38] S.M. Aminossadati, B. Ghasemi, A numerical study of mixed convection in a horizontal channel with a discrete heat source in an open cavity, European Journal of Mechanics-B/Fluids, (2009) 590-598.

[39] A.I. Alsabery, F. Selimefendigil, I. Hashim, A.J. Chamkha, M. Ghalambaz, Fluid-structure interaction analysis of entropy generation and mixed convection inside a cavity with flexible right wall and heated rotating cylinder, International journal of heat and mass transfer, (2019) 331-345.

[40] H.K. Hamzah, Q.R. Al-Amir, A. Abdulkadhim, S.Y. Ahmed, F.H. Ali, A.M. Abed, I.M. Abed, In a vented square enclosure, the effect of a flexible baffle attached to a solid cylinder on mixed convection, Arabian Journal for Science and Engineering, (2022) 15489-15504.

[41] H. Saleh, Z. Siri, I. Hashim, Role of fluid-structure interaction in mixed convection from a circular cylinder in a square enclosure with double flexible oscillating fins, International Journal of Mechanical Sciences, (2019) 105080.

[42] D.T. Yaseen, M.A. Ismael, Analysis of power law fluid-structure interaction in an open trapezoidal cavity, International Journal of Mechanical Sciences, (2020) 105481.

[43] L .Wang, Z. Chai, , & Shi, B, Regularized lattice Boltzmann simulation of double-diffusive convection of power-law nanofluids in rectangular enclosures; International Journal of Heat and Mass Transfer, (2016) 381-395.

[44] L .Wang, C. Huang, , X. Yang, Z. Chai, Z., & Shi, B, Effects of temperature-dependent properties on natural convection of power-law nanofluids in rectangular cavities with sinusoidal

temperature distribution, International Journal of Heat and Mass Transfer, (2019) 688-699.

[45] O. Benhizia, M. Bouzit, Natural convection of power-law fluid in a horizontal annulus between outer cylinder and inner flat tube, International Journal of Thermofluid Science and Technology(2023) Volume 10, Issue 4, Paper No. 100402